Article

An Alternative Method for the Generation of Consistent Mapping to Monitoring Land Cover Change: A Case Study of Guerrero State in Mexico

René Vázquez-Jiménez [1], Raúl Romero-Calcerrada [2,*], Rocío N. Ramos-Bernal [1], Patricia Arrogante-Funes [3] and Carlos J. Novillo [3]

1   Cuerpo Académico UAGro CA-93 Riesgos Naturales y Geotecnología, FI, Research Group on Technologies for Landscape Analysis and Diagnosis (TADAT), Universidad Autónoma de Guerrero, Av. Lázaro Cárdenas s/n, CU, 39070 Chilpancingo, Guerrero, Mexico; rvazquez@uagro.mx (R.V.-J.); rnramos@uagro.mx (R.N.R.-B.)
2   Research Group on Technologies for Landscape Analysis and Diagnosis (TADAT), Facultad de Ciencias Jurídicas y Sociales, Universidad Rey Juan Carlos, Paseo de los Artilleros s/n., Vicálvaro, 28032 Madrid, Spain
3   Research Group on Technologies for Landscape Analysis and Diagnosis (TADAT), Departamento de Tecnología Química y Ambiental, ESCET, Universidad Rey Juan Carlos, C/Tulipán s/n, Móstoles, 28933 Madrid, Spain; patricia.arrogante@urjc.es (P.A.-F.); carlos.novillo@urjc.es (C.J.N.)
*   Correspondence: raul.romero.calcerrada@urjc.es

Abstract: Land cover is crucial for ecosystems and human activities. Therefore, monitoring land cover changes has become relevant in recent years. This study proposes an alternative method based on conventional change detection techniques combined with maximum likelihood (MaxLike) supervised classification of satellite images to generate consistent Land Use/Land Cover (LULC) maps. The novelty of this method is that the supervised classification is applied in an earlier stage of change detection exclusively to identified dynamics zones. The LULC categories of the stable zones are acquired from an initial date's previously elaborated base map. The methodology comprised the use of Landsat images from 2011 and 2016, applying the Sun Canopy Sensor (SCS + C) topographic correction model enhanced through the classification of slopes, using derived topographic corrected images with NDVI, and employing Tasseled Cap (TC) Brightness-Greenness-Wetness indices and Principal Components (PCs). The study incorporated a comparative analysis of the consistency of the LULC mapping, which is generated based on control areas. The results show that the proposed method, although slightly laborious, is viable and fully automatable. The generated LULC map is accurate and robust and achieves a Kappa concordance index of 87.53. Furthermore, the boundary consistency was visually superior to the conventional classified map.

Keywords: land use/land cover (LULC); LULC mapping; image classification; change detection

1. Introduction

Only a third of the Earth's surface is covered by land (approximately 140 million km^2) [1]. Forest ecosystems help maintain biological diversity, water cycle regulation, carbon storage, and other ecological functions [2,3]. Some of the main causes of biodiversity loss are land cover change and anthropogenic disturbances, including the degradation or intensification of land use [4,5]. The transformation of forests into agricultural or urban areas has become common in the last 30 years in several regions of Mexico [6–8]. Every year, 0.3% of Mexico's vegetation surface is transformed and undergoes a LULC change [9].

Due to population growth, half of the world's native forest cover has been lost, and 30% of the ecosystems have been destroyed irreversibly [10,11]. These changes degrade the soils and alter the microclimate at local scales. In the short term, more significant concerns are modified ecosystem functions and services, and associated disruption of human well-being (i.e., forest ecosystem services such as water availability, food production, climate regulation, recreation, and culture) [11–13]. These issues have put the governments of

various countries on alert. In addition, the United Nations has recognized that nature is under increasing stress due to deforestation and desertification caused by human activities and climate change. These pose significant challenges to sustainable development and have affected millions of lives. Hence, sustainable development goals were set to manage forests, combat desertification, mitigate land degradation, and prevent biodiversity loss [14].

The need to develop scientific studies on the dynamics of LULC is widely recognized and aims to assess the magnitude, causes, and consequences within the coupled human and natural systems (CHANS). These studies are in demand mainly in tropical countries such as Mexico, which has a high concentration of natural and cultural wealth and has simultaneously recorded high ecosystem loss and degradation [15].

LULC mapping through Remote Sensing techniques and GIS provides essential support to monitor and evaluate LULC transitions [16–19]. These land cover maps are helpful to scientists, land managers, policy decision-makers, and end-users involved with environmental problems or sustainable land resources [20,21]. The importance of providing land cover maps has become more urgent as environmental monitoring programs accelerate and concerns about our changing environment increase. Data sources, methods, and technologies help deduce the consequences of degradation processes, desertification, decreased biodiversity, and natural and cultural loss. Thus, possible patterns and future behavior could be explored in applied regions, and the subsequent consequences can be anticipated. This data can be very useful in designing and planning conservation and territorial management.

Thematic mapping (e.g., LULC) is an essential input for ecosystem characterization and the study of evolutionary dynamics through time and space. The study of ecological processes at the landscape scale is based on the indexes estimated from land cover classifications [22–24]. Thematic cartography is commonly used but is not free from errors associated with the limited ability to discern the optical image capture systems themselves (remote sensors) [25], which causes confusion between specific map categories. These errors and related confusions are more likely to occur in regions of high levels of biodiversity (such as Mexico) with many LULC thematic classes categorized on maps.

At global and regional scales, several land cover datasets derived from remotely sensed data are available (for example, the MODIS Land Cover product [26], Global Land Cover 2000 [27], and Glob Cover produced by the European Space Agency (ESA) [28]). However, some studies showed disagreement between the global land cover datasets [29,30]. Other works were published about the reliability of regional LULC mapping. Laba et al., 2002 [31] and Wickham et al., 2004 [32] evaluated maps prepared in the year 1992 in the USA, analyzing 29 thematic classes of the Gap Analysis Project (GAP) and 21 classes of the National Land Cover Data (NLCD). Wulder et al., 2007 [33] published the reliability of the Vancouver Island map in Canada prepared in the year 2000 for 18 thematic classes considered in the Earth Observation for Sustainable Development (EOSD) program. The above studies exhibit numerous discrepancies among classes in the analyzed maps in the order of 38% to 70% global consistency.

The reliability of the thematic map used in the studies concerning changes in LULC is essential to the quality of findings. Otherwise, these spatial or thematic errors can be detrimental to the monitoring, characterization, and modeling of LULC changes. Supervised classification is commonly used in remote sensing to generate reliable LULC maps. This requires land cover sample and ground-truth data, which are necessary to assign each class according to the spectral data of the satellite images or the derived transformation images. Ground-truth integration is often a complicated and expensive task that involves exceptional processing, time, and resources. In addition, the ground-truth data must be accurate enough (in space, but especially in time) to represent the reality of cover categories. However, in ecosystem monitoring and land cover dynamics studies, the necessary historical ground-truth data are often unavailable [34].

Furthermore, in spatial and temporal reports, the border consistency of each class is transcendent to quantify the change. Some possible variations could be due to inconsistent

interpretation by the classification model of the analyzed data. This inconsistency causes temporal alterations in factors such as changes in vegetation health, differences in lighting due to different geometries of the sun and sensor, and the sensor data record [35,36]. Consequently, these would generate errors in the spatial boundaries of categories, and hence, some of the changes observed by comparing LULC maps of different years may be due to the mentioned artifacts, which cause errors in defining category boundaries or identification [37,38] and alter the evaluation results of land cover change.

To overcome this fact, we proposed an alternative method to generate spatial and thematics consistent LULC mapping at a local or regional scale through combined remote sensing techniques. First, a LULC base map of an initial date was built by supervised classification. Second, change detection is applied between the initial and final dates, and another supervised classification is applied exclusively to the identified changed zones. Finally, the LULC map of the final date is constructed by acquiring the covers of the initial base map of the non-changed zones and integrating it with the classified zones of detected changed areas.

This study proposes additional specialized work, such as data collection, processing, and analysis. However, satellite imagery offers advantages such as free remotely sensed data (Landsat, Sentinel, ASTER, among others.). Some of the other advantages are that satellite imagery represents the temporal data in different electromagnetic spectral bands (multispectral data), the temporal resolution of freely available sensors (16 days, average), and the spatial resolution of images in the visible and infrared bands (Landsat 30 m, Aster 15–30 m, Sentinel 10–20 m) is suitable for local or regional scale studies.

2. Materials and Methods

In this section, we explain the proposed methodology step by step. To facilitate an understanding of the approach and the assessment of the results, it is applied here in the central zone of Guerrero State in Mexico as a study case.

2.1. Study Area

The study area is in the central zone of Guerrero State in Mexico. It covers 4800 km^2, located in a mountainous region with elevations ranging from 480 m to 2960 m above the mean sea level (Figure 1).
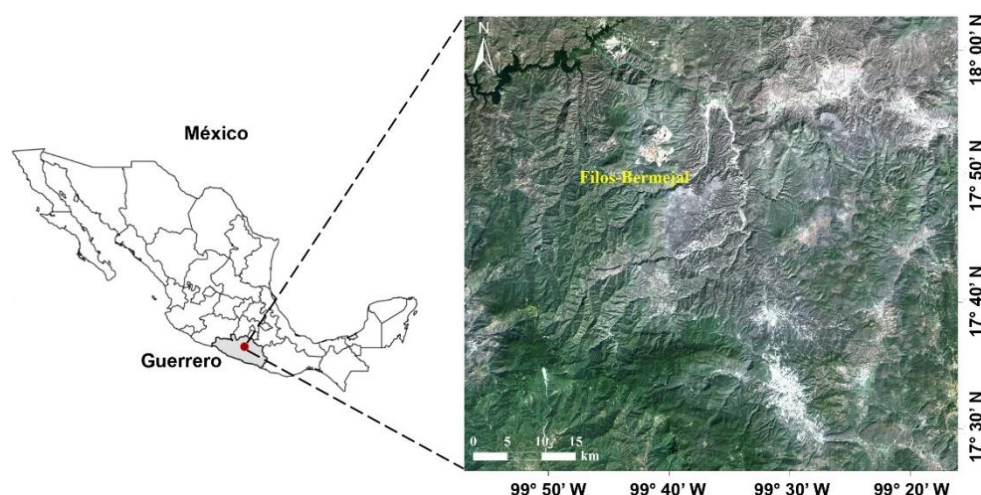
Figure 1. Study area: The central zone of Guerrero State in Mexico.

The temperature ranges were between 19.7 °C and 24.2 °C, recorded in December and May, respectively. The area is covered by 43.8% of forest (coniferous, mesophilic, and mixed), 39.3% of deciduous forest, 8.2% of agricultural and livestock use, 6.7% of induced vegetation, 1.7% of human settlements and urban areas, 0.2% of water bodies, and 0.1% of bare ground [39]. According to the 2010 Census, there are 308 towns in the study area,

which comprise 296 rural (less than 2500 inhabitants) and 12 urban towns. There were 84,835 inhabited homes and 363,938 inhabitants ($\approx$75.7 inhabitants per km^2) with 48.2% men and 51.8% women [40].

The study area identified diverse triggering and conditioning factors, such as pres-sure on the forest or agricultural areas, risk areas due to natural phenomena such as flooding and landslides, and anthropic actions. Another identified factor was clandestine logging and increasing deforestation due to industrial mining activity. The Filos-Bermejal mining corridor, located in the area, is the largest gold deposit in Latin America and is projected to extract more than 60 million tons of gold over 20 years [41]. This activity has impacted the local ecosystems, intensified the LULC change dynamics, and impacted landscape transformation (Figure 2).

Figure 2. Mining in the study area. (**a**,**b**) Exploitation front at the El Tajo, Filos-Bermejal mine. (**c**) Waste reservoir, Jales dam.

The study attempted to represent the pressure exerted by social and natural agents on local ecosystems, which prevail in many world regions. The method proposed here could be applied to similarly affected regions. Therefore, the study is globally relevant in its approach and use and is initially applied locally.

2.2. Methods

The methodological design (Figure 3) for elaborating a consistent LULC mapping proposal is based on five steps.

Vector mapping of land use and vegetation, series II (1993) to V (2011) was used in this study, and along with the official cartographic maps, was provided by the National Institute of Statistics and Geography (INEGI). Local experts on the integration and development of local and regional ecosystems (academy and government agencies) were consulted to define the vegetation and land covers under the temporal and spatial scale relevant to the study area. The defined LULC values are shown in Table 1.
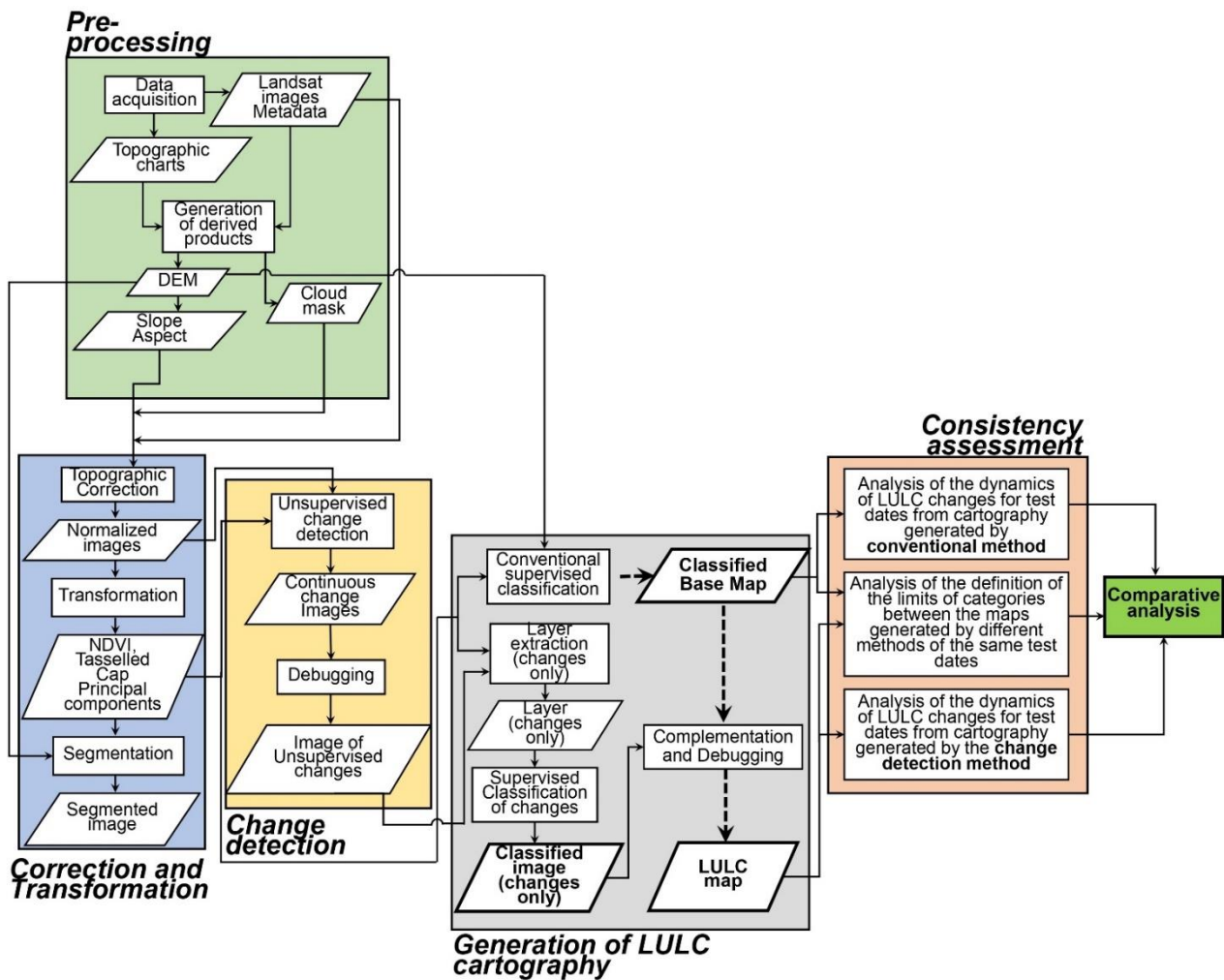
Figure 3. General flowchart of the proposed methodology.

Table 1. Definition of the legend's categories of LULC for the performance of the classification stage.

Id	Description
1-1	Encino forest
1-2	Pine forest
1-3	Mixed forest
2-1	Deciduous forest
3-1	Agricultural area
4-1	Bare soil
5-1	Water bodies
6-1	Urban/Industrial Areas

2.2.1. Pre-Processing

A 30-m grid digital elevation model (DEM) was used, based on topographic maps of scale 1:50,000, courtesy of INEGI. From the DEM, maps of the angular slopes and terrain orientation (Aspect) were generated.

Two Landsat surface reflectance (SR) images were used (Path 26, Row 48, WRS-2), acquired from the U.S. Geological Survey Earth Resources Observation and Science Center (USGS-EROS), which were offered as Climate Data Records (CDR) [42,43] with a spatial resolution of 30 m. One image was of the Landsat 5 Thematic Mapper (L5-TM) sensor from 24 February 2011, and another image was of the Landsat 8 Operational Land Imager (L8-OLI) sensor from 21 January 2016. Both dates correspond to the winter season in the northern hemisphere, a time of year, when the presence of clouds is significantly reduced in

the study area. In addition, the dates are close enough (in months) to be homogenized and avoid the detection of phenological changes derived from seasonal changes from winter to spring or summer, when there is an increase in rainfall and the quantity and vigor of the vegetation in the study area, mainly covered by Forest and Deciduous Forest. All bands were used, and cloud-shadow masks were generated for the images with clouds present.

2.2.2. Correction and Transformation

Topographic correction using the Sun Canopy Sensor + Correction (SCS + C) method was performed on each band and date to reduce the effect of slope changes on the reflectance values and the effect of terrain orientation and solar geometry at the time of image acquisition. The SCS + C method [44] is recommended for forested mountain areas over other land-based methods because it preserves the geotropic nature of the trees (typical to geoid growth) [45]. The C parameter used in topographic correction to moderate overcorrection of dimly illuminated pixels [46] was determined by linear regressions between the illumination and reflectance values and is based on the classification of topographic slopes of the studied area [47]. This improvement facilitates the detection of changes in the images and identifies the LULC classes in the classification stages.

With the topographically corrected bands, additional images were generated for each date through transformation processes, which employ normalized difference vegetation index (NDVI) [48], Tasseled Cap (TC) Brightness-Greenness-Wetness indices [49–51], and principal components (PCs) [22,49].

Furthermore, from the topographically corrected SR reflectance images, one more layer was generated by performing a segmentation process. The segmentation of satellite images is used to recognize spatial patterns and define their limits, aiming to simplify the image's representation in another image more meaningful and easier to analyze in subsequent processes. Segmentation divides the image into regions by identifying the contours using deterministic or stochastic intensity, color, or texture. Segmentation assigns a label to each pixel so that equal labels mean similar characteristics [52].

For this study, the watershed transformation method was applied to group pixels into image segments according to their spectral similarity. This method employs a similar approach to delineating a watershed to partition the input images based on their variance. Thus, a derived variance image is treated as a surface image that assigns pixels to particular segments based on their similarity [53].

The segmented image and the transformed images were used in the classification process to generate the LULC cartography.

2.3. LULC Map Generation

2.3.1. LULC Map Generation for the Base Date

One of the study dates was designated as the base (21 January 2016), and the conventional supervised maximum likelihood (MaxLike) classification process [22,54–56] was applied to generate a base LULC map. This process includes a sample of ground-truth information from the selected date. The layers used as input in the classification process were the first three PCs, the NDVI, and the DEM.

This process results in a classified image that must be debugged as it exhibits a speckled effect, also known as the salt-and-pepper effect, and is caused by high local spatial heterogeneity between neighboring pixels. As each pixel is dealt with in isolation from its neighbors in the pixel-based paradigm, close neighbors often have different classes despite being similar [57]. Thus, to overcome the speckle effect, a process of reducing this "salt-and-pepper noise" is conducted, which comprises reallocating isolated pixels in a category other than the one surrounding it [58]. This allows it to be included in the enveloping categories to improve the final LULC map.

To further reduce salt-and-pepper noise, the experts were consulted for their opinions to establish the recommended Minimum Mapping Unit (MMU) of the pixels that are grouped into different categories based on their integration into local ecosystems. The

MMU is considered to be adequately represented at a regional scale. We can conserve land cover classes that are sparse and fragmented, and they could be considerably misrepresented in the final land cover map [59]. The essential goal in selecting an appropriate MMU is to use as small a value as possible for the intended application of the classification while maintaining an acceptable level of accuracy [60]. The expert knowledge is very relevant to decide this relevant minimum area of each land cover class. Therefore, for the categories with large areas (forest and deciduous forest), it was proposed that the groups of pixels that were reassigned to enveloping classes were those groups with a size smaller than 18,000 m^2 (20 pixels). Alternately, for the rest of the classified image categories (agricultural areas, bare soil, water bodies, and urban/industrial areas), the idea was to debug groups of pixels smaller than 9000 m^2 (10 pixels). Figure 4 shows the process of LULC mapping generation of the base date.
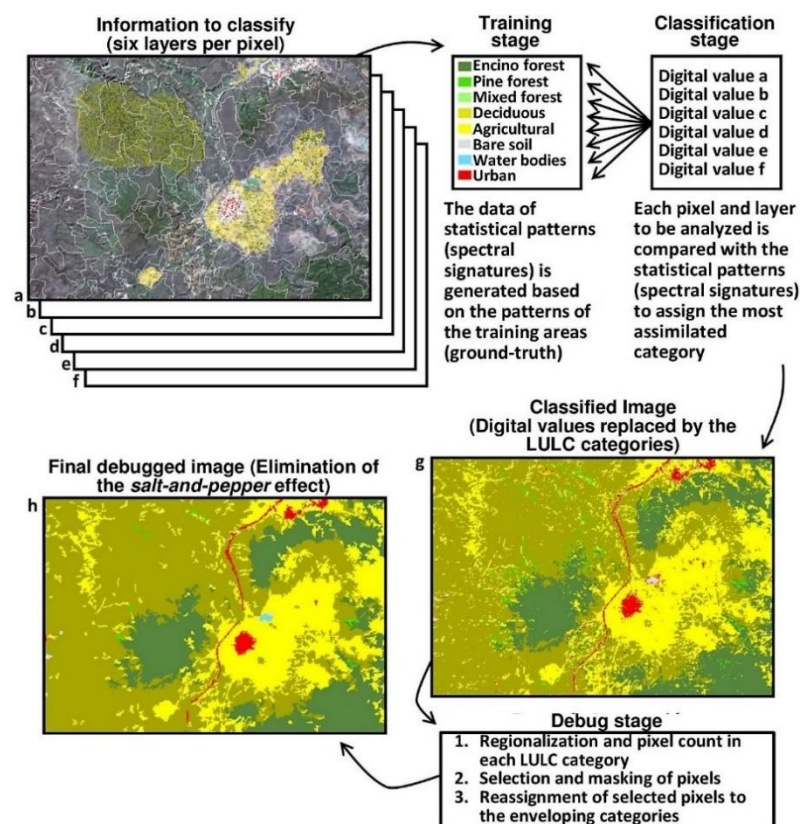
Figure 4. Overview process of supervised MaxLike classification and the LULC map for the base date. Classified layers: (**a**) Segmented image, (**b**–**d**) First three PCs, (**e**) NDVI, (**f**) DEM, (**g**) resulting image from classification, and (**h**) Final image.

2.3.2. LULC Map Generation for the Test Date

To generate the LULC map corresponding to the test date (24 February 2011), a supervised MaxLike classification process was applied exclusively to the change zones identified in the previous detection stage. Ground-truth data of the stable pixels (no-change) corresponding to the base date were used as training data for classification. This was done in accordance with the change detection results, which revealed that these areas temporally maintained the same LULC.

The unclassified areas, which correspond to the no-change pixels that resulted from the earlier detection process, complemented the LULC data from the base date map. It was assumed that these areas were unchanged during the analysis period so that the LULC would remain the same on both dates.

Figure 5 shows the proposed methodology for the test date LULC map generation.
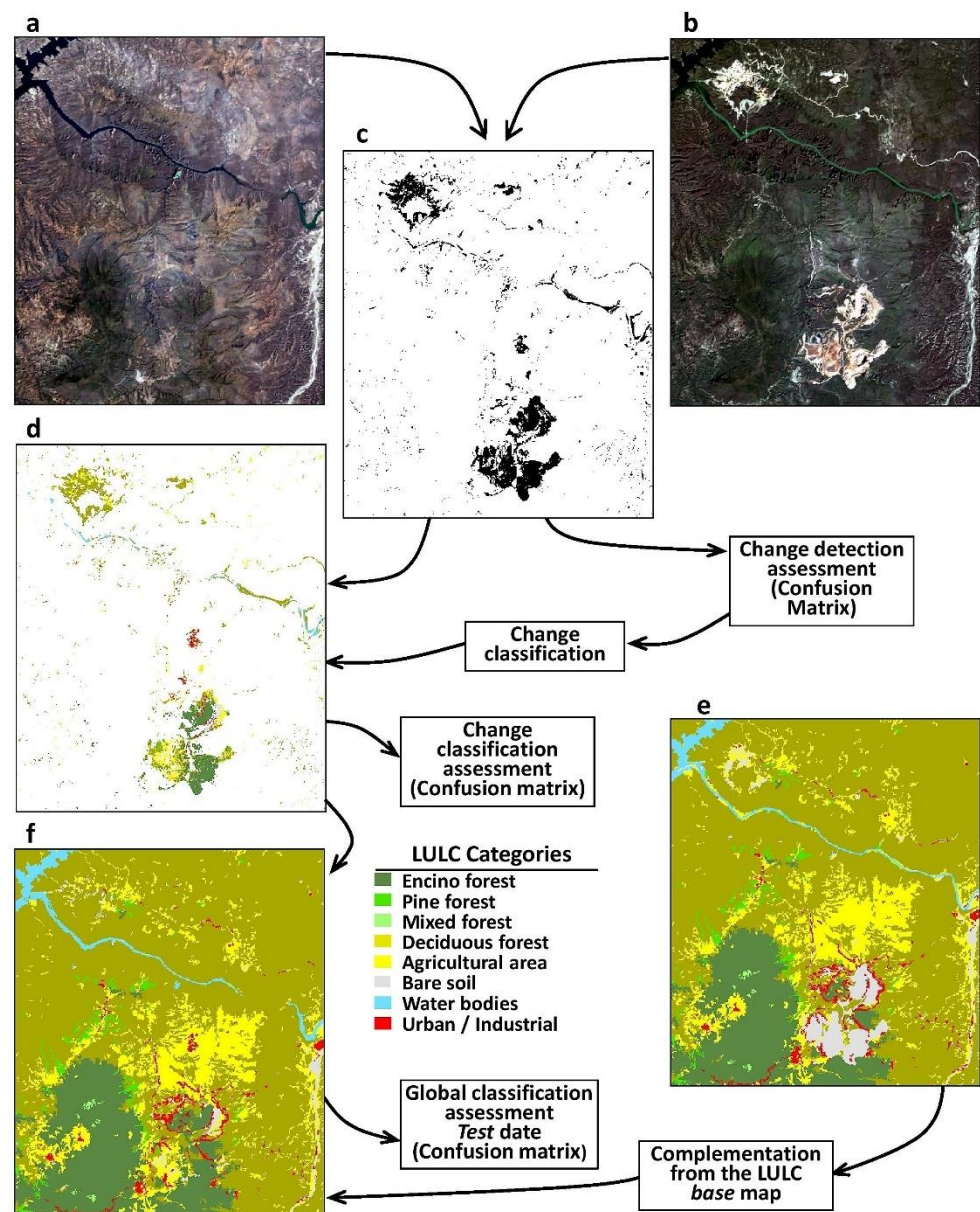
Figure 5. Test date LULC map (generated through change detection). (**a**) Test date image, (**b**) Base date image, (**c**) Change detection map, (**d**) Classification of the change detected pixels, (**e**) Base LULC map, and (**f**) Final test date LULC map.

The process is initiated with two images: the base date (Figure 5b) and the test date (Figure 5a). The images are used for change detection with linear regression (LR) [35,61,62] using the first PCs images as input and obtaining continuous change detection through images (residual) for the analysis period. According to a threshold value, a final thematic map was generated that isolated the pixels in change/no-change categories created by segmenting the residual image. Thus, the changed areas can be distinguished from those that remained unchanged, as shown in Figure 5c. Following Hervás and Rosin [63], the threshold was automatically defined by selecting the value that corresponds to the point in the histogram distribution where the maximum perpendicular line intersects with the secant line between the highest and lowest points of the residual image histogram [64].

Following the proposed method, the pixels matching the map of changes were extracted from the test date data (the first three PCs, the NDVI, and the DEM) and used as input in the classification process to generate a LULC map of the changed zones (Figure 5d).

As mentioned earlier, the ground-truth information from the base date of non-changed areas was used in the classification to train the model under the following conditions: first, it corresponds to the unchanged pixels in the analysis period. Second, the LULC remains unchanged in theory, and third, image dates correspond to the same seasonal period. Thus, the base date ground-truth data could theoretically be used to train a classification to the same base date or any unchanged test date area for the change detection task.

To complement the areas that were not classified (no-change), the LULC data were acquired from the base date (Figure 5e). The image resulting from the classification and complementation tasks was debugged to eliminate the salt-and-pepper effect, to finally obtain the test date LULC map (Figure 5f).

2.4. Accuracy Assessment

Any cartographic producer will ensure that they generate a product of the highest quality. Nevertheless, unfortunately, any cartographic product is not error-free. For example, in Europe, CORINE Land cover has a geometric accuracy better than 100 m and Thematic accuracy better than 85% (https://land.copernicus.eu/pan-european/corine-land-cover, accessed on 2 June 2021). In other words, thematic accuracy has a 15% error. For this reason, it is essential to assess the quality of produced maps.

To assess the accuracy of the classification process, 262 polygons were digitized and identified as ground-truth data. By interpreting a color aerial photo slide close to the base date and aided by the LULC official maps, 434,339 pixels were identified in their corresponding LULC category (Table 1). For classification and subsequent validation, these pixels were randomly separated into two groups. The first consisted of 289,559 pixels (2/3 of the ground-truth), which were reserved for use in the classification model. The second consisted of 144,780 pixels (1/3 of the ground-truth) and were reserved for assessing the classification accuracy of the process. The last subgroup of ground-truth samples was compared with the final classification map through confusion matrices to obtain the omission and commission errors.

The Kappa concordance coefficient of agreement [65] was obtained to quantify the difference between the observed map-reality agreement and the randomly expected agreement. The Kappa index attempts to define the degree of adjustment due to the categorization accuracy without considering the causes of random factors [66]. The Kappa coefficient was calculated as follows:

$$k = (n \sum_{i=1,n} X_{ii} - \sum_{i=1,n} X_{i+} X_{+i}) / (n^2 - \sum_{i=1,n} X_{i+} X_{+i}) \tag{1}$$

where k is the Kappa coefficient of agreement, n is the sample size, X_{ii} is the observed agreement, and X_{i+} X_{+i} is the expected agreement in each category i.

The Kappa coefficient allows us to determine whether the marked degree of agreement draws away or is not significantly different from the expected random agreement. The agreement is highlighted in the diagonal of the confusion matrix, and the expected agreement is used to calculate the fit between the map and reality due to randomness [22].

To assess the accuracy of the change detection process, events that have caused changes in the LULC were explicitly identified in the study area, such as deforestation, increasing bare soil areas by mining, landslides, flooding, and fires, among others. Areas were also identified wherein the LULC remains unchanged with similar characteristics, such as forests, bare soils, and urban areas. Thus, a sampling of 90 polygons was identified as ground-truth data, and their pixels were categorized as change and unchanged. By interpreting colored, aerial photo slides close to the study dates, aided and with the help of official LULC maps, and considering the reclassification of the categories of interest, samples of covers representative of the polygons were identified, selected, and digitized that in the photographs coincide with the characteristics defined for the classes sought to be incorporated into the ground-truth data; 7523 pixels were defined as changed and 7612 pixels as unchanged (Figure 6). These ground-truth data were compared with the

final thematic maps obtained from the detection process and applying the thresholding technique through confusion matrices to obtain the omission and commission errors.
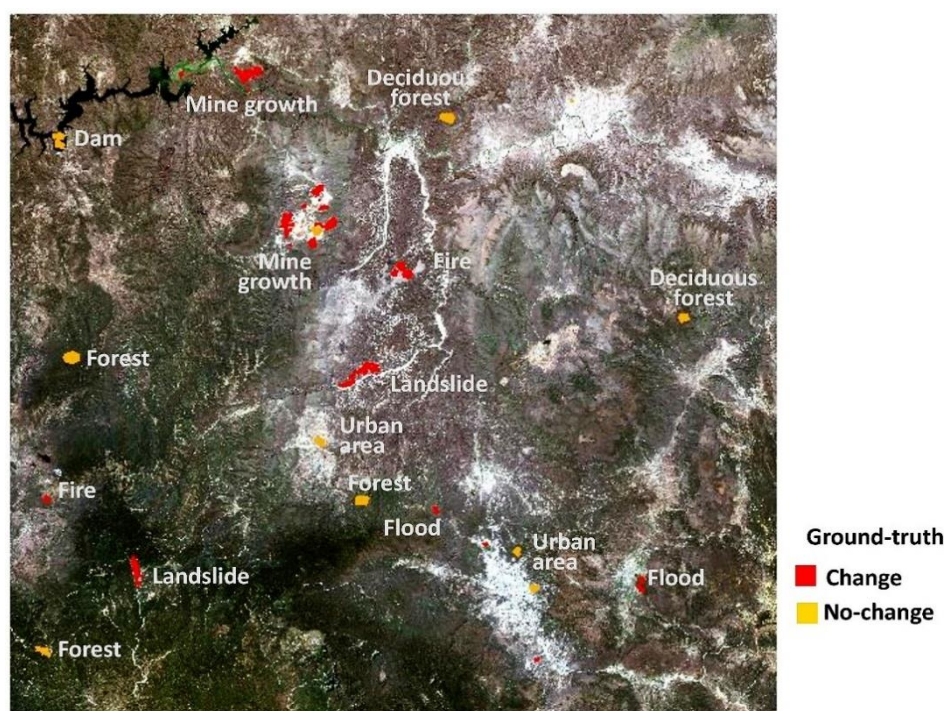
Figure 6. Spatial distribution of ground-truth polygons over the study area. The categories change (in red) and Non-change (in yellow) are shown during the 2011–2016 period.

As seen in Figure 5, it was possible to generate the LULC map of the test date from the proposed method by using ground-truth data from another base date to train the classification model without any specific ground-truth information for the test date. However, samples of ground-truth polygons were integrated for the test date with the help of LULC official maps exclusively for validating the proposed methodology. Thus, 232 polygons were sampled as ground-truth, 429,529 pixels were identified in their corresponding LULC category (Table 1), and randomly separated into two groups. The first comprised 284,030 pixels (2/3 of the ground-truth), and the second comprised 142,055 pixels (1/3 of the ground-truth). As per the resulting map of the change detection task, the last group was simultaneously divided into two subgroups. One corresponds to the ground-truth for the change zones and the other for the unchanged zones. The first subgroup was used to assess the classification accuracy applied to the changed areas (Figure 5d). To validate the final LULC map (Figure 5f), the sampled group of 142,055 pixels was compared with the final LULC map through confusion matrices to obtain the omission and commission errors, and the Kappa concordance coefficient.

Ground-truth information available for the test date is used to validate the proposed methodology. A conventional MaxLike classification was performed on the test date, using the group of 284,030 pixels in the training stage. This resulting conventional LULC map was compared with the LULC map generated by the proposed method using change detection.

Earlier studies have reported the minimum representativeness of the interest categories required for classification processes, which range from $n + 1$ [67], $10n$ [68] to $100n$ [69], where n is the number of bands that integrate the classification analysis [22]. While integrating the ground-truth data used in classification training and stages of date validation, the representativeness remains intact and exceeds the minimum number of pixels used in the sample criteria mentioned.

3. Results and Discussion

3.1. Base Date LULC Map

Figure 7 shows the true-color composition of the base date image, the supervised classification results, and classification with the reduced salt-and-pepper noise processes.
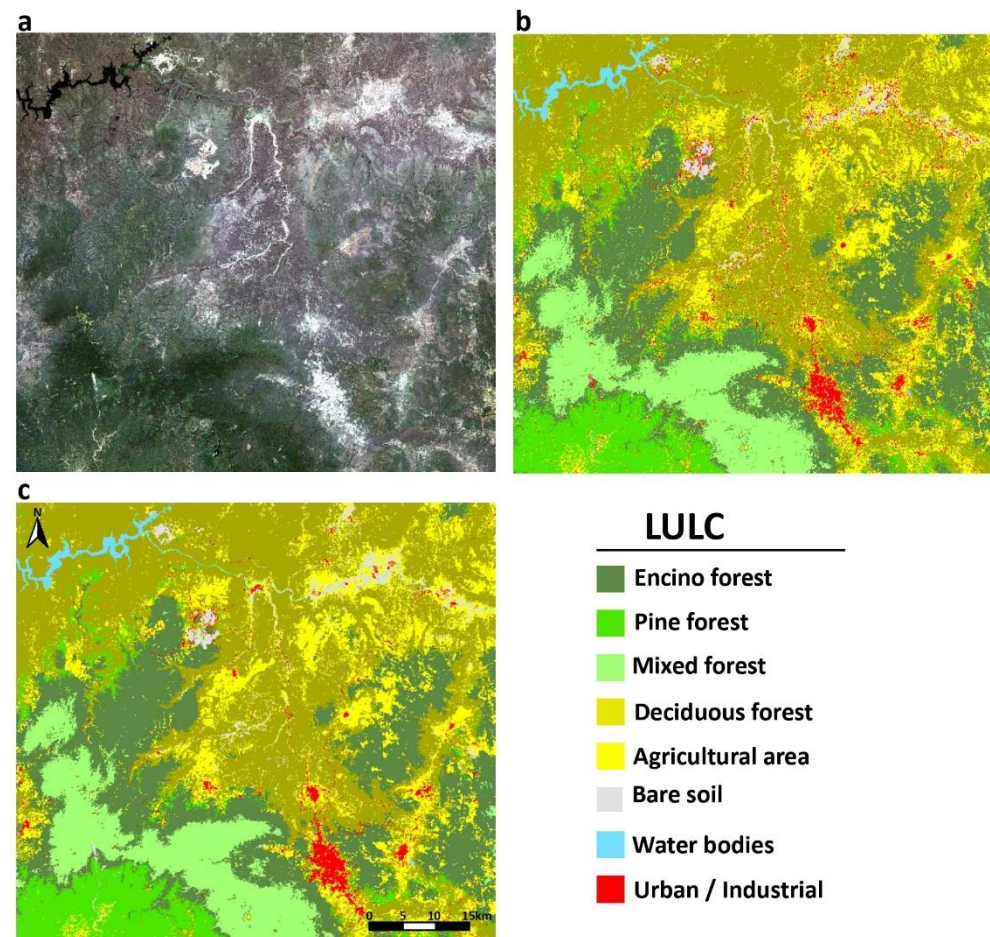
Figure 7. Base date. (**a**) True-color composition image (RGB bands), (**b**) Classified image, and (**c**) Classified image with the reduced salt-and-pepper noise.

The general LULC of the study area can be observed in the true-color composition (Figure 7a). Some pixels are categorized in isolation from the training data used (salt-and-pepper noise) in the classified image. These are bare soil pixels (in gray) classified in isolation as an urban area (in red) due to their similarity (Figure 7b). The presence of many salt-and-pepper noise occurrence of isolated pixels with high local spatial heterogeneity between neighboring pixels demonstrated why it was necessary to correct it in the land cover classification [58]. The improvement through the reduced salt-and-pepper noise process can be observed in Figure 7c. The image resulting from the supervised classification with the reduced salt-and-pepper noise (Figure 7c) represents the LULC map used as a base for the test date map generation.

The layers used as input in the classification process were the first three PCs of remote sensing bands, the NDVI, and the DEM. Principal Component Analysis (PCA) and Independent Component Analysis (ICA) are different methods. Principal Component Analysis (PCA) is very frequently used in remote sensing. PCA is a statistical technique used to feature extraction and data reduction. In our study, we wished to obtain fewer bands that integrate the information of the other bands.

However, Independent Component Analysis (ICA) is not yet often used in land cover change or remote sensing in general. ICA is a different technique use to recovering

unobserved data on multispectral bands, exploiting only the assumption of mutual independence. ICA could improve the quality of the classification [70–72]. For this reason, in the future, we will develop and evaluate new methodologies incorporating IC bands.

Accuracy Assessment of the Base Date LULC Map

The correspondence between land covers shown in the true-color composition (Figure 7a), and the final LULC map can be appreciated. However, a quantitative evaluation was developed by comparing the categories of LULC obtained by the classification with the reduce salt-and-pepper noise process with the ground-truth reserved for validating of the base date through a confusion matrix (Table 2).

Table 2. Confusion matrix of the final base date LULC map compared with the ground-truth reserved for the validation stage.

LULC	Encino Forest	Pine Forest	Mixed Forest	Decid. Forest	Agric.	Bare Soil	Water Bodies	Urban/Indust.	Total	User Match	Comm Error
Encino forest	22,082	426	2333	881	87	0	4	0	25,813	85.5	14.5
Pine forest	1277	17,001	187	1222	95	0	0	0	19,782	85.9	14.1
Mixed forest	480	14	31,045	0	0	0	0	0	31,539	98.4	1.6
Decid. forest	442	243	0	34,477	3102	1	0	12	38,277	90.1	9.9
Agric.	197	154	13	2090	12,203	6	8	580	15,251	80.0	20.0
Bare soil	17	8	0	18	181	1689	24	105	2042	82.7	17.3
Water bodies	0	0	0	0	0	0	3450	0	3450	100.0	0.0
Urban/ Indust.	0	0	0	4	312	73	5	8232	8626	95.4	4.6
Total	24,495	17,846	33,578	38,692	15,980	1769	3491	8929	144,780		
Produc. Match	90.1	95.3	92.5	89.1	76.4	95.5	98.8	92.2			
Omission errors	9.9	4.7	7.5	10.9	23.6	4.5	1.2	7.8		**Kappa**	**87.64**

Most of the pixels reserved for the validation stage are concentrated in the main diagonal of the confusion matrix, which ensures good results in allocating the classification categories. However, some discrepancies are observed, which need to be analyzed outside the diagonal.

It is observed that some pixels identified in the ground-truth data as Encino forest are designated as pine forest (5.2%) in the classification model. Opposite instances are also observed, i.e., 2.4% of the pixels identified as "pine forest" are classified as "encino forest," and 6.9% of the pixels identified as "mixed forest" are classified as "encino forest". Deciduous forest cover occupies an extensive and dispersed area in the study area, and discrepancies are also observed here. We observed that of the total pixels identified in the ground-truth data as deciduous forest, 2.3% are classified as Encino, 3.2% as pine, and 5.4% as agricultural areas. Similarly, opposite discrepancies are observed, wherein 19.4% of the pixels identified as agricultural areas are classified as deciduous forests. According to the global values of the confusion matrix, bare soils, and water bodies are correctly assigned by the classification model, while of the total pixels identified in the ground-truth data as urban/industrial areas, 6.5% are wrongly classified as agricultural areas.

The discrepancies observed in the LULC base map are relatively normal because forests and deciduous forest classes cover large areas and are surrounded by other forest cover types that make class delineation difficult while processing.

Certain types of land cover have similar structures and properties, and hence, they react in similar ways to energy [44,73], i.e., some crops in agricultural areas can easily be confused with low vegetation, which is characteristic of deciduous forests. Hence, they are wrongly assigned to that category. Another case is that some areas were identified as agricultural areas in the ground-truth data, although they were uncultivated (fallow) at the image acquisition time. Similarly, soils in the classification process are categorized as urban/industrial areas because both categories have a similar spectral response (high reflectance values).

These discrepancies lead to additional efforts in integrating ground-truth data, increasing the resources, and preparation time needed to attain the required quality for this kind of study. These efforts are justified for obtaining the desired definition for LULC base maps.

The confusion matrix analysis indicates that the omission errors are low, registering 8.8% on average for the analyzed LULC. The highest value is 23.6% due to the discrepancies between the agricultural and deciduous forests (Table 2). Commission errors are also low, registering 10.2% for the analyzed LULC, with the highest records (20.0%) corresponding to agricultural areas. These values are consistent with the earlier works in similar LULC conditions, which report ≈22% [74]. These low values of omission and commission errors indicate that the producer and user match success records are high (average of ≈90%), except for agricultural land cover that records ≈78% of success in matching pixels due to the discussed discrepancies (Table 2).

According to the confusion matrix, the accuracy of the LULC map date test was considered satisfactory and reached a Kappa concordance index of 87.64%. It was also concluded that the designation of the final map is appropriate and validates the performance of the proposed method for LULC map generation for the test date image without its ground-truth data.

3.2. Test Date LULC Map

3.2.1. Change Detection Map

As mentioned earlier, the LULC map generation proposal for the test date starts with an LR change detection performance using the first PCs from the test and base dates as input images and thresholding technique, which results in a continuous image by the automatic secant method [75].

Figure 8 shows the result of the process of detecting changes between the test and base dates.
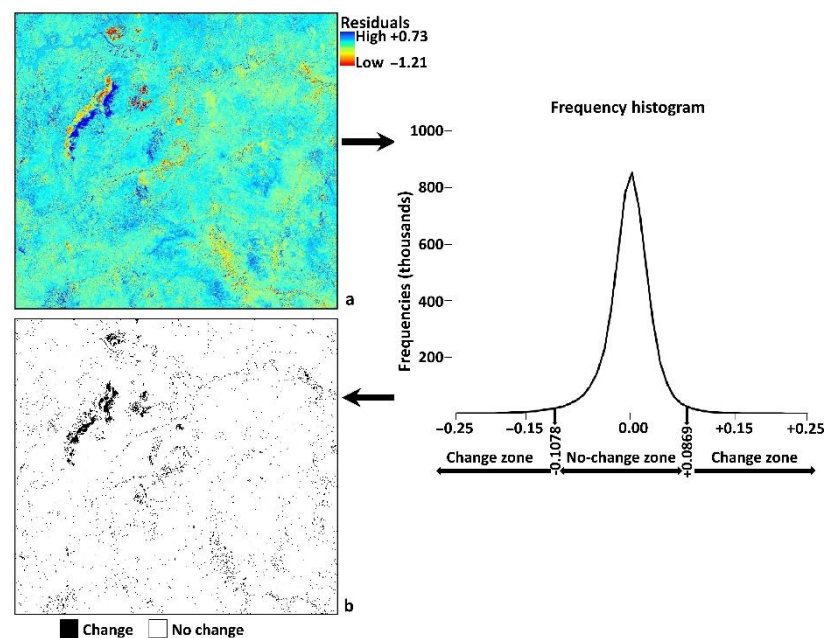
Figure 8. Change detection process by LR of the first PCs. (**a**) Image of continuous change (residual), (**b**) Thematic map of change obtained by thresholding the residuals by the secant method.

The image of continuous change (residuals) is obtained by applying the LR change detection method to the first PCs images (Figure 8a) between the base and test dates, and the ranges of the residual values are represented in the histogram. The frequency distributions are typical, with average values close to zero ($-8.25 \times 10-14$), close to the residual values representing stable zones.

Chen et al. 2012 [55] developed a similar method to update the classification map of five land cover classes only for changed areas. Their results and accuracy are analogous to our outcome. Xian et al. 2009 [76] proposed a similar technique using a change vector analysis (CVA) to detect changed areas. The detected changed areas were reclassified in the end using decision tree classification (DTC). Their technique is similar in accuracy to the proposed method and is cost-effective. According to Chen et al. 2003 [77], the input images used in the change detection technique acquired in different years must correspond to the same phenological period to avoid commission errors when applying the CVA change detection method.

The threshold values were −0.1078 and +0.0869, determined by the secant method, and the thematic change map recorded a 2.86% change ratio (Figure 8b). Thus, our proposed method establishes suitable thresholds automatically. This is an advantage concerning the CVA applied by Xian et al. 2009 [76], in which a single CVA threshold seems to be inappropriate for identifying the area of different change types.

The resulting change thematic map (Figure 8b) was subjected to an evaluation based on the confusion matrix, as shown in Table 3.

Table 3. Confusion matrix of the change thematic map compared with the Change/No-change ground-truth.

Condition	No-Change	Change	Total	User Match	Commission Error
No-change	74,192	1216	8708	85.6	14.0
Change	120	6307	6424	98.1	1.9
Total	7612	7523	15,135		
Producer Match	98.4	83.8			
Omission errors	1.6	16.2		**Kappa**	**82.33**

According to the confusion matrix, the average omission error is 8.87%, while the commission error is 7.92%. Thus, a Kappa concordance index of 82.33% is reached.

The change detection method applied in this stage was LR using the first PCs (Figure 8b). It is known that LULC classes react differently to energy [78,79]. Hence, the images used in processing also react differently for the type of data contained. Therefore, modifying either the change detection method or the input data would mean relatively different results of change pixel ratios, commission and omission errors, and a different Kappa concordance index. However, we assumed that the results from the method and applied input are sufficiently robust. Although, this could be the context for future study that explores the improvement of the applied change detection method.

3.2.2. Classification of Change Zones

Figure 9 shows the classification result, using the layers of extracted data corresponding to those pixels detected as change.

The resulting image from the classification was submitted to an evaluation that employed a confusion matrix between the resulting LULC categories and the test date ground-truth pixels, which match the pixels in the thematic change map. Table 4 shows the confusion matrix.
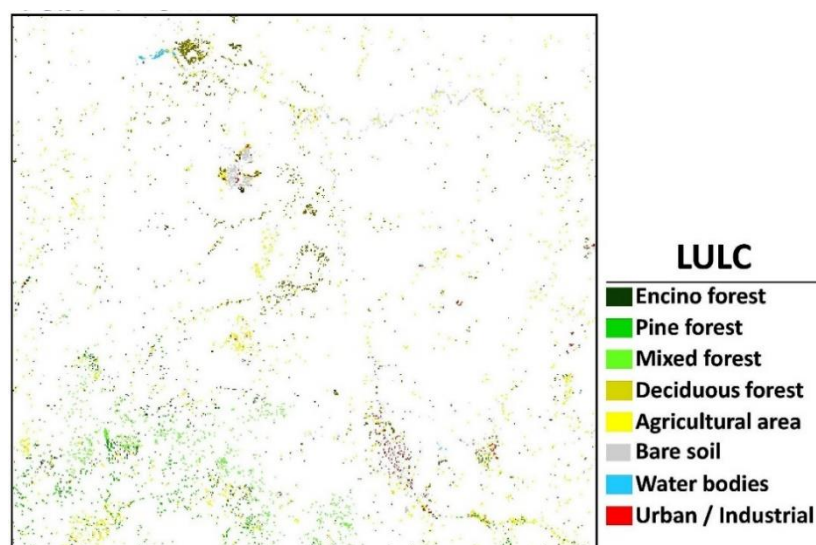
Figure 9. Result of the classification of the exchange areas obtained for the test date.

Table 4. Confusion matrix of the LULC change-classified map compared with the ground-truth of the test date.

LULC	Encino Forest	Pine Forest	Mixed Forest	Decid. Forest	Agric.	Bare Soil	Water Bodies	Urban/Indust.	Total	User Match	Comm. Error
Encino forest	60	10	9	0	8	0	0	0	87	69.0	31.0
Pine forest	1	316	13	0	88	0	0	0	418	75.6	24.4
Mixed forest	2	15	372	0	0	0	0	0	389	95.6	4.4
Decid. forest	3	10	15	108	22	0	0	2	160	67.5	32.5
Agric.	8	29	11	28	1669	18	3	6	1772	94.2	5.8
Bare soil	1	0	2	10	116	758	17	125	1029	73.7	26.3
Water bodies	0	0	0	0	0	0	90	0	90	100.0	0.0
Urban/ Indust.	3	0	0	2	121	15	11	482	634	76.0	24.0
Total	78	380	422	148	2024	791	121	615	4579		
Produc. Match	76.9	83.2	88.2	73.0	82.5	95.8	74.4	78.4			
Omission errors	23.1	16.8	11.8	27.0	17.5	4.2	25.6	21.6		**Kappa**	**79.03**

Most of the pixels reserved for assessing the classification of change zones are concentrated in the main diagonal matrix. However, it is observed that the deciduous forest had an omission error of 27% because of the pixel discrepancies between the agricultural, soil, and urban covers. A similar issue is observed with water bodies, where 25.6% of the pixels are confused between agricultural, bare soil, and urban areas. However, globally, there is a balance between commission and omission errors, with 18.6% and 18.5% values, respectively, and an average success of ≈82% for both producer and user matches.

The resulting classification of the image (Figure 9) constitutes an essential part of the proposed methodology. The supervised classification is carried out on pixels identified as changes by a previous detection task, wherein the data layers from the test date were trained with ground-truth data corresponding to the base date. This methodology would mainly allow supervised classification to be applied to one date using training data of another date as long as the data is common and homogeneous temporally and is based on change detection exercise.

3.2.3. Complementation of the Test Date LULC Map

Figure 10 shows the result of the complementation task on the classification of change detection (Figure 9) with data from the LULC base map (Figure 7c).
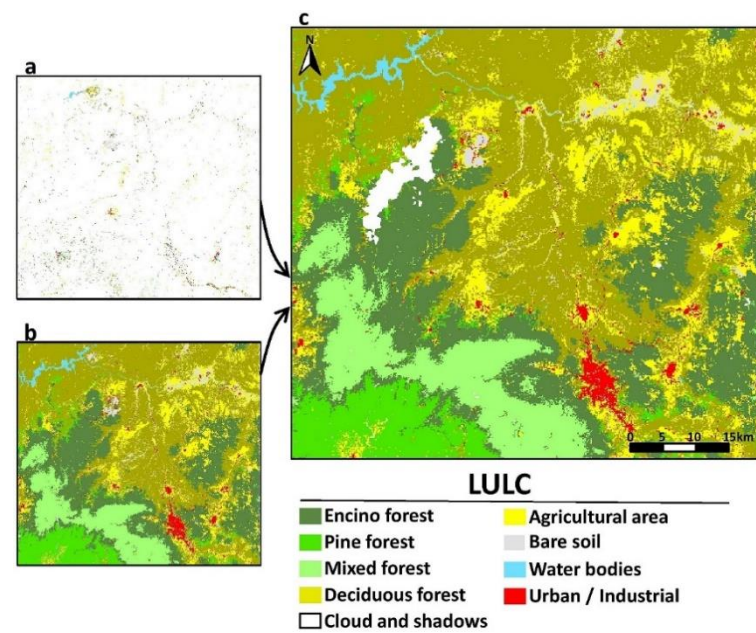
Figure 10. Integration of the test date LULC map. (**a**) Classification of changed pixels, (**b**) base date LULC map, (**c**) test date LULC final map, supplemented and corrected for the salt-and-pepper effect.

3.2.4. Accuracy Assessment of the LULC Test Date Map

Similar to earlier cases, the accuracy assessment of the test date LULC map integrated by the proposed methodology was carried out using the confusion matrix as shown in Table 5.

Table 5. Confusion matrix of the test date LULC through change-detection map compared with the ground-truth data.

LULC	Encino Forest	Pine Forest	Mixed Forest	Decid. Forest	Agric.	Bare Soil	Water Bodies	Urban/Indust.	Total	User Match	Comm Error
Encino forest	20,110	638	2229	853	75	0	5	0	23,910	84.1	15.9
Pine forest	1057	21,403	182	1225	97	0	0	0	23,964	89.3	10.7
Mixed forest	516	14	27,297	0	0	0	0	0	27,827	98.1	1.9
Decid. forest	536	211	0	32,636	3120	20	1	2	36,526	89.4	10.6
Agric.	141	187	27	2160	14,963	44	9	388	17,919	83.5	16.5
Bare soil	6	11	0	7	230	1670	30	86	2040	81.9	18.1
Water bodies	0	0	0	0	0	0	3594	0	3594	100.0	0.0
Urban/Indust.	7	0	0	5	270	109	15	5869	6275	93.5	6.5
Total	22,373	22,464	29,735	36,886	18,755	1843	3654	6345	142,055		
Produc. Match	89.9	95.3	91.8	88.5	79.8	90.6	98.4	92.5			
Omission errors	10.1	4.7	8.2	11.5	20.2	9.4	1.6	7.5		**Kappa**	**87.53**

The confusion matrix is similar to those presented earlier. The omission error average was 9.2%, while the average of the commission errors was 10.0%. The matrix reports ≈91% for producer and ≈90% for user match. Thus, the LULC map generated by classification by detecting changes for the test date is considered satisfactory and reaches a Kappa concordance index of 87.53%.

3.3. Consistency Assessment

3.3.1. Conventional LULC Map vs. LULC Map through Change Detection

An official map for the test date was available to integrate ground-truth information, which allowed a conventional MaxLike supervised classification.

Figure 11 shows the test date LULC map using conventional classification. The official LULC map corresponds to the same reference year for the 2011 test date, including the LULC map generated through change detection.
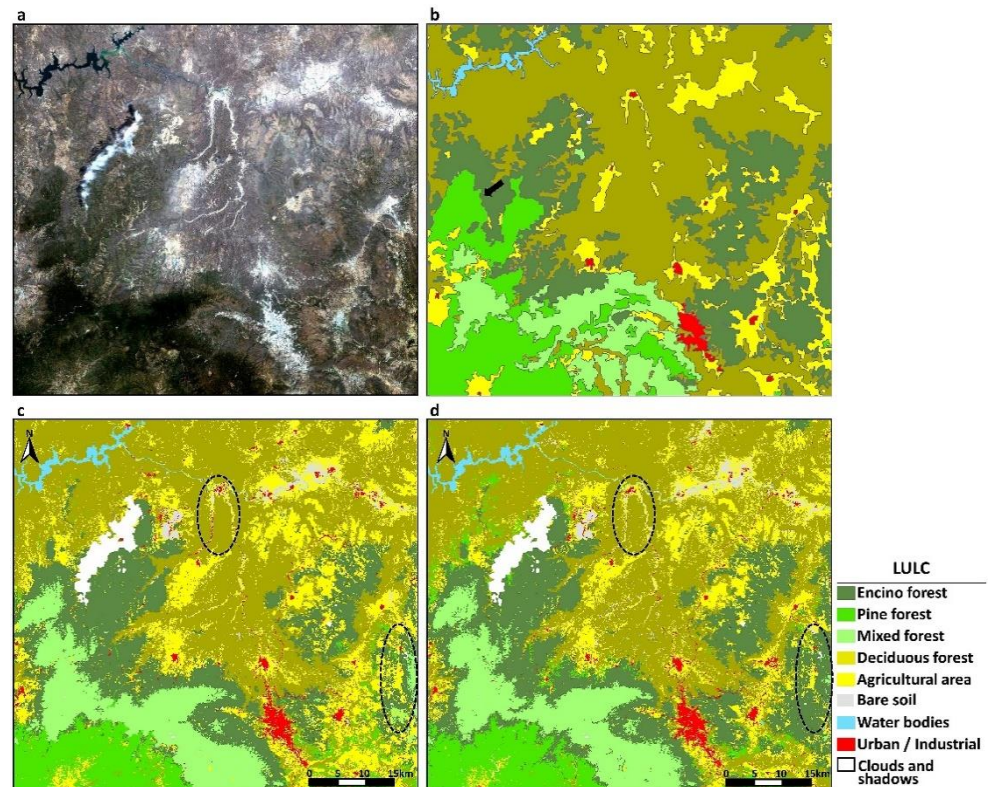
Figure 11. Classifications applied to the test date (2011). (**a**) RGB True-color composition, (**b**) LULC Official cartography of the test date study area (INEGI, 2015), (**c**) Conventional classification image applying own training polygons (2011), and (**d**) Classification image through change detection for 2011, applying training polygons of the base date (2016).

Correspondence between the true-color image (Figure 11a), the official LULC mapping (Figure 11b), and the LULC maps generated by the conventional classifications (Figure 11c) and through change-detection is observed (Figure 11d). Some differences were noted in detail in the official LULC mapping generated by the classifications. For instance, the lack of continuity in the river area, the absence of the exploitation area of the mine, and the discrepancies in the classes of characterized forests (as indicated by the arrow in Figure 11b).

For the LULC maps obtained by conventional classification (Figure 11c) and by classification through change detection (Figure 11d), it is observed that the configuration presents similar results. However, some differences were also identified (those indicated with a black dotted line), such as the discrepancies between bare soil and urban areas (in red in the center of the images) and the wrong classification of Encino forest as mixed forest (in the lower right part of the images).

The test date LULC map generated by a conventional classification was subjected to an accuracy evaluation through a confusion matrix. This resulted in average omission and commission errors of 6.6% and 8.2%, respectively, and these values generated high successes of both producer ($\approx$93%) and user match ($\approx$92%). Therefore, according to the confusion matrix values, the evaluation of the accuracy of LULC categories by the conventional classification of the test date (2011) is considered satisfactory and reaches a Kappa concordance index of 91.18%.

Table 6 shows the key indicators resulting from the classifications applied to the test date.

Table 6. Summary of the leading indicators of the confusion matrices applied for assessing the LULC maps generated by conventional classification and through change detection, applied to the test dates (2011), and evaluated with same-date ground-truth data.

Indicator	Change Classification (Partial Evaluation)	Conventional Classification	Classification Via Change Detection
		(Global Evaluation)	
Omission error	18.5	6.6	9.2
Commission error	18.6	9.2	10.0
Kappa index	79.03	91.18	87.53

In the accuracy assessment applied to the different LULC maps generated for the test date (Table 6), the partial evaluation indexes improve when the images are complemented and submitted to the global evaluation. This is because the base date data used to complement the unclassified areas have undergone prior treatment and evaluation, improving the quality. Hence, all data and corresponding quality are acquired from the global images integrated to generate the final LULC map.

Earlier, the results of the LULC maps generated by conventional classification and through change detection for the test date were visually explored, and similar results were indicated. However, some apparent differences observed, as shown in Figure 12, which shows the surfaces by category of the maps generated for the test date.
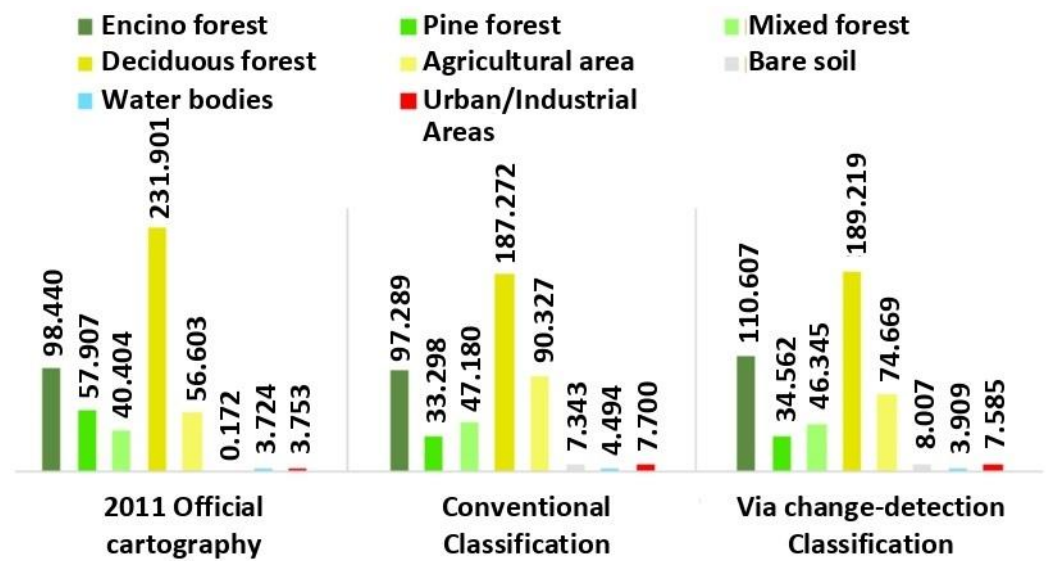
Figure 12. LULC surfaces of the generated maps by conventional methods and through change detection for the test date and the cartography LULC surfaces of 2011. Total surface: 474.904 hectares. Values in thousands of hectares.

The general trend is similar between the surface values of the compared maps. From Figure 12, most of the surface is identified as deciduous forest, surface minorities are identified as bare soil, and water bodies as urban areas since maps generally coincide.

Figure 13 showcases the LULC maps generated for the test date. Differences in the definition of the limits of the LULC categories are evident in results as those shown enclosed in dotted lines marked in Figure 12. This variation of boundaries generated simultaneously is observed in the cross-tabulation matrix of the LULC maps performed for the test date, as shown in Table 7.
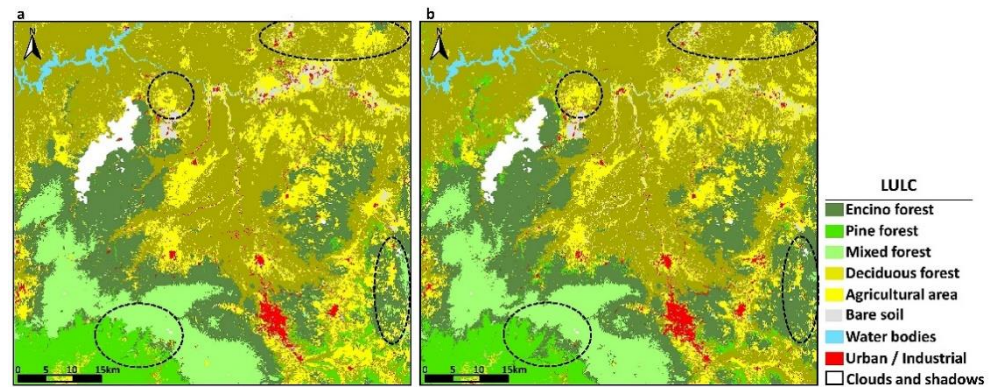
Figure 13. LULC maps from test date (2011), resulting from (**a**) conventional classification methods and (**b**) change detection methods.

Table 7. Cross tabulation matrix of the LULC maps generated for the test date comparing the applied methods. Values in % about the total area of the LULC categories of the conventional map.

2011 Via Change Detection	2011 Conventional Classification								2011 Via Change Detection	Difference (+)
	Encino Forest	Pine Forest	Mixed Forest	Decid. Forest	Agric.	Bare Soil	Water Bodies	Urban/ Indust.		
Encino forest	89.7	12.0	10.1	2.9	9.7	1.2	0.2	3.5	110,607.2	13.7
Pine forest	2.4	80.6	0.1	1.9	1.9	0.0	0.2	0.1	34,562.3	3.8
Mixed forest	3.9	0.2	89.9	0.0	0.1	0.1	0.0	0.1	46,344.6	1.8
Decid. forest	2.2	6.0	0.0	88.2	20.2	5.5	10.2	10.6	189,233.8	1.0
Agric.	1.6	1.0	0.0	6.4	64.2	22.9	1.0	15.4	74,669.0	17.3
Bare soil	0.0	0.1	0.0	0.4	2.0	61.3	3.2	9.2	8006.6	9.3
Water bodies	0.0	0.0	0.0	0.0	0.0	0.5	85.2	0.0	3895.2	13.4
Urban/ Indust.	0.1	0.1	0.0	0.2	1.9	8.4	0.1	61.0	7585.3	1.5
2011 Conventional	97,289.4	33,298.4	47,180.4	187,286.6	90,327.1	7325.3	4497.2	7699.7	474,904.0	
Difference	10.3	19.4	10.1	11.88	35.8	38.7	14.8	39.0		

In the main diagonal of the matrix, the surface percentage for each category of LULC matches in both maps, indicating the degree of similarity in the maps. However, three categories were observed (agricultural, bare land, and urban/industrial areas) that recorded more significant surface variations (marked in red) (Table 7).

From the main diagonal of the matrix, each category of LULC surface percentage is shown through change detection, and the LULC map represents an approximate surface for different categories. Most correspond to moderate changes (less than ≈10%), although significant gains or losses are observed for the previously indicated categories (marked in green) (Table 7).

The proposed alternative method, termed change detection, is considered appropriate for spatial and temporal studies to generate LULC mapping. The method's main advantage is that it allows dispensing ground-truth data for a test date, which in theory provides greater availability of information (base date data). Each stage of the method has a coherent and robust approach and is wholly based on the consolidated theoretical frameworks of remote sensing.

3.3.2. LULC Dynamics Based on Conventional Classification Methods

An analysis of the dynamics of LULC was performed between the test date and the base date and was based exclusively on the LULC maps generated from conventional classification. The analysis reveals that supervised classifications performed using the conventional method resulted in satisfactory evaluations through the Kappa concordance index that is oriented to evaluate successes and commission and omission errors only for

areas that were covered with ground-truth samples reserved for the accuracy assessment stage. Thus, following the conventional method, the Kappa index is extrapolated to the entire resulting image. The conventional process is repeated for another analysis date in a multi-temporal analysis and yields similar results, as shown in Figure 14.
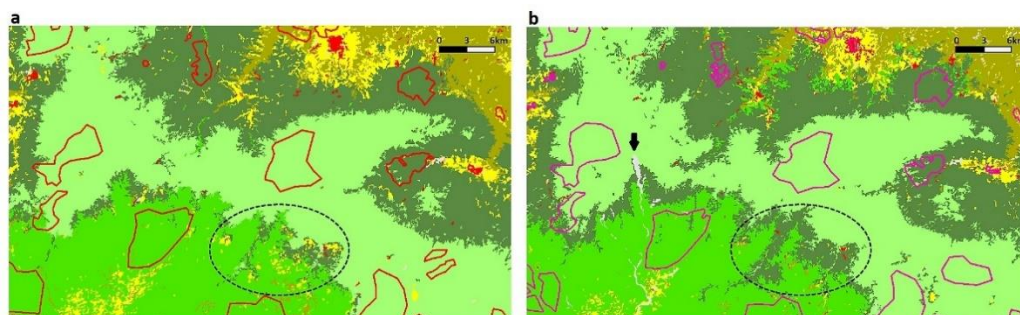
Figure 14. LULC maps generated by the conventional supervised classification method applied to (**a**) the test (2011) and (**b**) base (2016) dates. Ground-truth polygons are included.

For these classifications, Kappa indices were obtained of 91.18% for 2011 and 87.64% for 2016, which are acceptable. The results were similar or better than those of other similar studies [30]. However, from the changes observed in the maps resulting in the definition of boundaries (surrounded by black dotted line) and consequent analyses and discussions, a reasonable doubt arose, if the changes and boundaries definition observed in the LULC map obtained with the conventional classification, could correspond to real gradual changes (such as the landslide indicated by arrow), or may be attributed to a different spectral interpretation by the classifying algorithm from one date to another, which could be derived from any of the other factors, and hence, not be a real change of LULC.

Strictly based on the Kappa concordance index obtained from conventional classifications performed under similar conditions, it would be pertinent to take both conventional classifications as valid. However, a different way of assigning a thematic category was applied by the classification algorithm. Hence, an erroneous assessment of the changes could be obtained since thematic errors on any of the dates would generate changes that are not real and would be reflected in the quantification of the surfaces, which could lead to overestimation of land cover loss in one direction, and simultaneously produce a false increase in another sense [15].

For the benefit of the proposed method, we affirm that the generation of LULC mapping through change detection initially determined the areas on which the supervised classification should be applied, which corresponded to zones detected as change, and retained the rest of the zones as stable and therefore unchanged in the LULC. Naturally, this method affects the maps created and the analysis of the dynamics of LULC changes due to the uniformity introduced in the defining limits of LULC.

4. Conclusions

Land cover cartography is essential to scientists and land managers to monitor biodiversity, natural resources, and understand the dynamic environment [15,20,21]. Therefore, it is necessary to have a homogeneous, reliable, and comparable mapping for LULC dynamics studies. In land cover change studies, comparing LULC maps of different years may produce spatial or thematic artifacts and land cover boundaries errors [37,38].

Our methods produce temporal and thematic consistent Land Cover maps that reduce errors in the spatial boundaries of land cover classes, coherent thematic category boundaries, or identification and alter the evaluation results of land cover change.

The use of confirmed zones of change may provide uniformity and certainty of the spatial limits and thematic land cover class for the LULC maps. Finally, our methodology allows us to focus on change areas, optimizing time and resources because those areas are

really small. A smaller surface can optimize the workload and time of production: we need fewer control points, we can choose better control points, we reduce the workload, we have greater control in verification, among other benefits.

The applied change detection method has a particular application in the automatic definition of the threshold value by limiting human participation and adding objectivity and speed. Furthermore, the threshold is a critical stage that defines the global capacity of the model. Thus, an appropriate threshold maximizes the ability of the method to differentiate the dynamic (changes) from the stable areas (no-changes).

The proposed change detection as an alternative method is appropriate for spatial and temporal studies to generate LULC mapping. The dispensing of ground-truth data for any date is beneficial for optimum utilization of resources and time. Furthermore, it would be impossible to apply any conventional supervised method without having the corresponding ground-truth data due to a lack of historical data with sufficient quantity or quality. This further highlights the benefits of this method.

The findings suggest and open a new line to improve change detection techniques, strengthen and optimize the applied methods, and give new methods to detect much broader ranges of change found in the present study.

Author Contributions: Conceptualization, R.V.-J. and R.R.-C.; methodology, R.V.-J. and R.R.-C.; validation, R.V.-J., R.R.-C., R.N.R.-B., P.A.-F. and C.J.N.; investigation, R.V.-J., R.R.-C., R.N.R.-B., P.A.-F. and C.J.N.; writing—original draft preparation, R.V.-J., R.R.-C., R.N.R.-B., P.A.-F. and C.J.N.; writing—review and editing, R.V.-J., R.R.-C., R.N.R.-B., P.A.-F. and C.J.N. All authors have read and agreed to the published version of the manuscript.

Conflicts of Interest: The authors declare no conflict of interest.

References

1. PNUMA. *Perspectivas del Medio Ambiente Mundial 2002 GEO-3: Pasado, Presente y Futuro*; Mundi-Prensa: Madrid, Spain, 2002.
2. Sombroek, W.G.; Sims, D. *Planning for Sustainable Use of Land Resources: Toward a New Approach (FAO Land and Water Bulletin 2)*; Food and Agriculture Organization of the United Nations: Rome, Italy, 1995.
3. Wood, S.; Sebastian, K.; Scherr, S.J. *Pilot Analysis of Global Ecosystems: Agroecosystems, a Joint Study by International Food Policy Research Institute and World Resources Institute*; International Food Policy Research Institute and World Resources Institute: Washington DC, WA, USA, 2000.
4. Lambin, E.F. Modelling and monitoring land-cover change processes in tropical regions. *Prog. Phys. Geogr.* **1997**, *21*, 375–393. [CrossRef]
5. Turkelboom, F.; Poesen, J.; Trébuil, G. The multiple land degradation effects caused by land-use intensification in tropical steeplands: A catchment study from northern Thailand. *Catena* **2008**, *75*, 102–116. [CrossRef]
6. del Carmen Salazar, E.; Zavala, J.; Castillo, O.; Cámara, R. Evaluación espacial y temporal de la vegetación de la Sierra Madrigal, Tabasco, México (1973–2003). *Investig. Geogr.* **2004**, 7–23. Available online: http://www.scielo.org.mx/scielo.php?script=sci_arttext&pid=S0188-46112004000200002 (accessed on 11 July 2021).
7. Landa, R.; Meave, J.; Carabias, J. Environmental deterioration in rural Mexico: An examination of the concept. *Ecol. Appl.* **1997**, *7*, 316–329. [CrossRef]
8. Velázquez, A.; Mas, J.F.; Díaz Gallegos, J.R.; Mayorga-Saucedo, R.; Alcántara, P.C.; Castro, R.; Fernández, T.; Bocco, G.; Ezcurra, E.; Palacio, J.L. *Patrones y Tasas de Cambio de Uso del Suelo en México*; Gaceta Ecológica: Ciudad de México, México, 2002; pp. 21–37, ISSN 1405-2849.
9. Victoria, H.A.; Niño, A.M.; Rodriguez, A.J.A. *La Serie IV De Uso Del Suelo Y Vegetación Escala 1:250,000 De INEGI, Información Del Periodo 2007–2008*; Instituto Nacional de Estadística y Geografía: Aguascalientes, México, 2013.
10. Curtis, P.G.; Slay, C.M.; Harris, N.L.; Tyukavina, A.; Hansen, M.C. Classifying drivers of global forest loss. *Science* **2018**, *361*, 1108–1111. [CrossRef] [PubMed]
11. Millennium Ecosystem Assessment. *Ecosystems and Human Well-Being: Synthesis*; Island Press: Washington, DC, USA, 2005.
12. Okruszko, T.; Duel, H.; Acreman, M.; Grygoruk, M.; Flörke, M.; Schneider, C. Broad-scale ecosystem services of European wetlands-overview of the current situation and future perspectives under different climate and water management scenarios. *Hydrol. Sci. J.* **2011**, *56*, 1501–1517. [CrossRef]
13. Rojas, A.M.; Ruiz-Agudelo, A.; Diazgranados, C.; Polanco, H.; Anderson, R.; Diazgranados, M.C. Approach to an integral valuation of mangrove's ecosystem services in a marine protected area. *Colomb. Pac. Region. J. Environ. Econ. Policy* **2019**, *8*, 322–342. [CrossRef]

14. United Nations. *Forests, Desertification and Biodiversity-United Nations Sustainable Development*; United Nations: New York, NY, USA, 2019; pp. 1–5.

15. Mas, J.-F.; Velázquez, A.; Couturier, S. La evaluación de los cambios de cobertura/uso del suelo en la República Mexicana. *Investig. Ambient.* **2008**, *1*, 23–39.

16. Corner, R.J.; Dewan, A.M.; Chakma, S. Monitoring and prediction of land-use and land-cover (LULC) change. In *Dhaka Megacity: Geospatial Perspectives on Urbanisation, Environment and Health*; Springer: New York, NY, USA; London, UK, 2014; pp. 75–97.

17. D'Aquino, P.; August, P.; Balmann, A.; Berger, T.; Bousquet, F.; Brondízio, E.; Brown, D.G.; Couclelis, H.; Deadman, P.; Goodchild, M.F. *Agent-Based Models of Land-Use and Land-Cover Change*; Report and Review of an International Workshop; LUCC International Project Office: Irvine, CA, USA, 2001; p. 124.

18. Soares-Filho, B.S.; Nepstad, D.C.; Curran, L.M.; Cerqueira, G.C.; Garcia, R.A.; Ramos, C.A.; Voll, E.; McDonald, A.; Lefebvre, P.; Schlesinger, P. Modelling conservation in the Amazon basin. *Nature* **2006**, *440*, 520–523. [CrossRef] [PubMed]

19. Verburg, P.H.; Kok, K.; Pontius, R.G.; Veldkamp, A. Modeling Land-Use and Land-Cover Change. In *Land-Use and Land-Cover Change. Global Change*; The IGBP Series; Lambin, E.F., Geist, H., Eds.; Springer: Berlin/Heidelberg, Germany, 2006; pp. 117–135. [CrossRef]

20. Aitkenhead, M.J.; Aalders, I.H. Automating land cover mapping of Scotland using expert system and knowledge integration methods. *Remote Sens. Environ.* **2011**, *115*, 1285–1295. [CrossRef]

21. Sutherland, W.J.; Adams, W.M.; Aronson, R.B.; Aveling, R.; Blackburn, T.M.; Broad, S.; Ceballos, G.; Cote, I.M.; Cowling, R.M.; Fonseca, G.A.B.D. One hundred questions of importance to the conservation of global biological diversity. *Conserv. Biol.* **2009**, *23*, 557–567. [CrossRef] [PubMed]

22. Chuvieco, E. *Teledetección Ambiental: La Observación de la Tierra Desde el Espacio*; Ariel Ciencia: Barcelona, Spain, 2010; p. 591.

23. Conde, M.C.; Perelman, S.B.; Cerezo, A. Efecto de diferentes métodos de clasificación de imágenes satelitales sobre índices de paisaje. *Rev. Teledetec.* **2009**, *32*, 5–13.

24. Smith, D.A. Online interactive thematic mapping: Applications and techniques for socio-economic research. *Comput. Environ. Urban. Syst.* **2016**, *57*, 106–117. [CrossRef]

25. Hartley, S.; Green, D.R. Integrating Photointerpretation and GIS for Vegetation Mapping: Some Issues of Error. In *Vegetation Mapping: From Patch to Planet*; Alexander, R., Millington, A., Eds.; John Wiley and Sons: New York, NY, USA, 2000; Chapter 7; pp. 03–134.

26. Friedl, M.A.; McIver, D.K.; Hodges, J.C.F.; Zhang, X.Y.; Muchoney, D.; Strahler, A.H.; Woodcock, C.E.; Gopal, S.; Schneider, A.; Cooper, A. Global land cover mapping from MODIS: Algorithms and early results. *Remote Sens. Environ.* **2002**, *83*, 287–302. [CrossRef]

27. Bartholome, E.; Belward, A.S. GLC2000: A new approach to global land cover mapping from Earth observation data. *Int. J. Remote Sens.* **2005**, *26*, 1959–1977. [CrossRef]

28. Arino, O.; Bicheron, P.; Achard, F.; Latham, J.; Witt, R.; Weber, J.L. GLOBCOVER: The most detailed portrait of Earth. *Eur Space Agency Bull.* **2008**, *2008*, 24–31.

29. Iwao, K.; Nishida, K.; Kinoshita, T.; Yamagata, Y. Validating land cover maps with Degree Confluence Project information. *Geophys. Res. Lett.* **2006**, *33*. [CrossRef]

30. Tchuenté, A.T.K.; Roujean, J.-L.; Jong, S.M.D. Comparison and relative quality assessment of the GLC2000, GLOBCOVER, MODIS and ECOCLIMAP land cover data sets at the African continental scale. *Int. J. Appl. Earth Obs. Geoinf.* **2011**, *13*, 207–219. [CrossRef]

31. Laba, M.; Gregory, S.K.; Braden, J.; Ogurcak, D.; Hill, E.; Fegraus, E.; Fiore, J.; DeGloria, S.D. Conventional and fuzzy accuracy assessment of the New York Gap Analysis Project land cover map. *Remote Sens. Environ.* **2002**, *81*, 443–455. [CrossRef]

32. Wickham, J.D.; Stehman, S.V.; Smith, J.H.; Yang, L. Thematic accuracy of the 1992 national land-cover data for the western United States. *Remote Sens. Environ.* **2004**, *91*, 452–468. [CrossRef]

33. Wulder, M.A.; White, J.C.; Magnussen, S.; McDonald, S. Validation of a large area land cover product using purpose-acquired airborne video. *Remote Sens. Environ.* **2007**, *106*, 480–491. [CrossRef]

34. Xie, Y.; Sha, Z.; Bai, Y. Classifying historical remotely sensed imagery using a tempo-spatial feature evolution (T-SFE) model. *ISPRS J. Photogramm. Remote Sens.* **2010**, *65*, 182–190. [CrossRef]

35. Singh, A. Review article digital change detection techniques using remotely-sensed data. *Int. J. Remote Sens.* **1989**, *10*, 989–1003. [CrossRef]

36. Vázquez-Jiménez, R.; Romero-Calcerrada, R.; Ramos-Bernal, R.N.; Arrogante-Funes, P.; Novillo, C.J. Topographic Correction to Landsat Imagery through Slope Classification by Applying the SCS C Method in Mountainous Forest Areas. *ISPRS Int. J. Geo Inf.* **2017**, *6*, 287–302. [CrossRef]

37. Mas, J.-F. Change estimates by map comparison: A method to reduce erroneous changes due to positional error. *Trans. GIS* **2005**, *9*, 619–629. [CrossRef]

38. Pan, X.; Zhao, J.; Xu, J. An object-based and heterogeneous segment filter convolutional neural network for high-resolution remote sensing image classification. *Int. J. Remote Sens.* **2019**, *40*, 5892–5916. [CrossRef]

39. INEGI. *Guía Para la Interpretación de Cartografía: Uso del Suelo y Vegetación: Escala 1:250,000, Serie V*; Instituto Nacional de Estadística y Geografía: Aguascalientes, Mexico, 2015; p. 195.

40. INEGI. *Censo de Población y Vivienda 2010*; Instituto Nacional de Estadística y Geografía: Aguascalientes, Mexico, 2011.

41. Universal, E. Excavan en Guerrero la Mina de Oro Más Grande de América Latina; México. 2005. Available online: https://www.cronica.com.mx/notas/2005/212974.html (accessed on 11 July 2021).

42. USGS. *Landsat 4-7 Climate Data Record (CDR) Surface Reflectance, Product Guide*; United States Geological Survey: Reston, VA, USA, 2015.
43. USGS. *Provisional Landsat 8 Surface Reflectance Product, Product Guide*; United States Geological Survey: Reston, VA, USA, 2015.
44. Soenen, S.A.; Peddle, D.R.; Coburn, C.A. A Modified Sun-Canopy-Sensor Topographic Correction in Forested Terrain. *IEEE Trans. Geosci. Remote Sens.* **2005**, *43*, 2148–2159. [CrossRef]
45. Gu, D.; Gillespie, A. Topographic normalization of Landsat TM images of forest based on subpixel sun–canopy–sensor geometry. *Remote Sens. Environ.* **1998**, *64*, 166–175. [CrossRef]
46. Teillet, P.M.; Guindon, B.; Goodenough, D.G. On the slope-aspect correction of multispectral scanner data. *Can. J. Remote Sens.* **1982**, *8*, 84–106. [CrossRef]
47. Vázquez-Jiménez, R.; Romero-Calcerrada, R.; Novillo, C.J.; Ramos-Bernal, R.N.; Funes, P.A. Applying the Chi-square transformation and automatic secant thresholding to Landsat imagery as unsupervised change detection methods. *J. Appl. Remote Sens.* **2017**, *11*, 016016. [CrossRef]
48. Lüdeke, M.K.B.; Ramage, P.H.; Kohlmaier, G.H. The use of satellite NDVI data for the validation of global vegetation phenology models: Application to the Frankfurt Biosphere Model. *Ecol. Model.* **1996**, *91*, 255–270. [CrossRef]
49. Baig, M.H.A.; Zhang, L.; Shuai, T.; Tong, Q. Derivation of a tasselled cap transformation based on Landsat 8 at-satellite reflectance. *Remote Sens. Lett.* **2014**, *5*, 423–431. [CrossRef]
50. Crist, E.P.; Cicone, R.C. A physically-based transformation of Thematic Mapper data-The TM Tasseled Cap. *IEEE Trans. Geosci. Remote Sens.* **1984**, 256–263. [CrossRef]
51. Healey, S.P.; Cohen, W.B.; Zhiqiang, Y.; Krankina, O.N. Comparison of Tasseled Cap-based Landsat data structures for use in forest disturbance detection. *Remote Sens. Environ.* **2005**, *97*, 301–310. [CrossRef]
52. Kaliyamurthie, K.P.; Parameswari, D. Remote Sensing Imaging for Satellite Image Segmentation. *Indian J. Sci. Technol.* **2015**, *8*. [CrossRef]
53. Angulo, J.; Serra, J. Segmentación de imágenes en color utilizando histogramas bi-variables en espacios color polares luminancia/saturación/matiz. *Comput. Sist.* **2005**, *8*, 303–316.
54. Ahmad, A.; Quegan, S. Analysis of Maximum Likelihood Classification on Multispectral Data. *Appl. Math. Sci.* **2012**, *6*, 6425–6436.
55. Chen, X.; Chen, J.; Shi, Y.; Yamaguchi, Y. An automated approach for updating land cover maps based on integrated change detection and classification methods. *ISPRS J. Photogramm. Remote Sens.* **2012**, *71*, 86–95. [CrossRef]
56. Verbovšek, T.; Popit, T. GIS-assisted classification of litho-geomorphological units using Maximum Likelihood Classification, Vipava Valley, SW Slovenia. *Landslides* **2018**, *15*, 1415–1424. [CrossRef]
57. Kelly, M.; Blanchard, S.D.; Kersten, E.; Koy, K. Terrestrial remotely sensed imagery in support of public health: New avenues of research using object-based image analysis. *Remote Sens.* **2011**, *3*, 2321–2345. [CrossRef]
58. Hirayama, H.; Sharma, R.C.; Tomita, M.; Hara, K. Evaluating multiple classifier system for the reduction of salt-and-pepper noise in the classification of very-high-resolution satellite images. *Int. J. Remote Sens.* **2019**, *40*, 2542–2557. [CrossRef]
59. Saura, S. Effects of minimum mapping unit on land cover data spatial configuration and composition. *Int. J. Remote Sens.* **2002**, *23*, 4853–4880. [CrossRef]
60. Knight, J.F.; Lunetta, R.S. An experimental assessment of minimum mapping unit size. *IEEE Trans. Geosci. Remote Sens.* **2003**, *41*, 2132–2134. [CrossRef]
61. Lu, D.; Mausel, P.; Brondízio, E.; Moran, E. Change detection techniques. *Int. J. Remote Sens.* **2004**, *25*, 2365–2401. [CrossRef]
62. Ridd, M.K.; Liu, J. A comparison of four algorithms for change detection in an urban environment. *Remote Sens. Environ.* **1998**, *63*, 95–100. [CrossRef]
63. Hervás, J.; Rosin, P.L. Tratamiento digital de imágenes de teledetección en el espectro óptico para el reconocimiento y control de deslizamientos. In Proceedings of the V Simposio Nacional Sobre Taludes y Laderas Inestables, Madrid, Spain, 27–30 November 2001; pp. 27–30.
64. Vázquez-Jiménez, R.; Ramos-Bernal, R.N.; Romero-Calcerrada, R.; Arrogante-Funes, P.; Tizapa, S.S.; Novillo, C.J. Thresholding Algorithm Optimization for Change Detection to Satellite Imagery. *Color. Image Proc.* **2018**. [CrossRef]
65. Cohen, J. A coefficient of agreement for nominal scales. *Educ. Psychol. Meas.* **1960**, *20*, 37–40. [CrossRef]
66. Couto, P. Assessing the accuracy of spatial simulation models. *Ecol. Model.* **2003**, *167*, 181–198. [CrossRef]
67. Schowengerdt, R.A. *Techniques for Image Processing and Classifications in Remote Sensing*; Academic Press: New York, NY, USA; London, UK, 2012.
68. Jensen, J.R. *Introductory Digital Image Processing: A Remote Sensing Approach*; Prentice Hall: Upper Saddle River, NJ, USA, 1996; Volume 7458.
69. Mather, P.M.; Koch, M. *Computer Processing of Remotely-Sensed Images: An Introduction*; John Wiley & Sons: New York, NY, USA, 2011.
70. Namdar, M.; Adamowski, J.; Saadat, H.; Sharifi, F.; Khiri, A. Land-use and land-cover classification in semi-arid regions using independent component analysis (ICA) and expert classification. *Int. J. Remote Sens.* **2014**, *35*, 8057–8073. [CrossRef]
71. Chignell, S.M.; Anderson, R.S.; Evangelista, P.H.; Laituri, M.J.; Merritt, D.M. Multi-Temporal Independent Component Analysis and Landsat 8 for Delineating Maximum Extent of the 2013 Colorado Front Range Flood. *Remote Sens.* **2015**, *7*, 9822–9843. [CrossRef]

72. Dabiri, Z.; Lang, S. Comparison of Independent Component Analysis, Principal Component Analysis, and Minimum Noise Fraction Transformation for Tree Species Classification Using APEX Hyperspectral Imagery. *Isprs Int. J. Geo Inf.* **2018**, *7*, 448. [CrossRef]

73. Justice, C.O.; Wharton, S.W.; Holben, B.N. Application of digital terrain data to quantify and reduce the topographic effect on Landsat data. *Int. J. Remote Sens.* **1981**, *2*, 213–230. [CrossRef]

74. Mora, T.J.G.; Mas, J.-F. Comparación de metodologías para el mapeo de la cobertura y uso del suelo en el sureste de México. *Investig. Geogr.* **2008**, 7–19. Available online: http://www.scielo.org.mx/scielo.php?script=sci_arttext&pid=S0188-46112008000300002 (accessed on 11 July 2021).

75. Hervás, J.; Barredo, J.I. Evaluación de la susceptibilidad de deslizamientos mediante el uso conjunto de SIG teledetección y métodos de evaluación multicriterio aplicación al barranco de Tirajana (Gran Canaria). In Proceedings of the V Simposio Nacional Sobre Taludes y Laderas Inestables, Madrid, Spain, 27–30 November 2001.

76. Xian, G.; Homer, C.; Fry, J. Updating the 2001 National Land Cover Database land cover classification to 2006 by using Landsat imagery change detection methods. *Remote Sens. Environ.* **2009**, *113*, 1133–1147. [CrossRef]

77. Chen, J.; Gong, P.; He, C.; Pu, R.; Shi, P. Land-use/land-cover change detection using improved change-vector analysis. *Photogramm. Eng. Remote Sens.* **2003**, *69*, 369–379. [CrossRef]

78. Richardson, A.J.; Wiegand, C.L. Distinguishing vegetation from soil background information. [by gray mapping of Landsat MSS data]. Photogramm. *Eng. Remote Sens.* **1977**, *43*, 1541–1552.

79. Song, C. Spectral mixture analysis for subpixel vegetation fractions in the urban environment: How to incorporate endmember variability? *Remote Sens. Environ.* **2005**, *95*, 248–263. [CrossRef]